






Article

Structural Investigation of Magnesium Complexes Supported by a Thiopyridyl Scorpionate Ligand

Matthew P. Stevens ¹, Emily Spray ¹, Iñigo J. Vitorica-Yrezabal ², Kuldip Singh ¹, Vanessa M. Timmermann ¹, Lia Sotorrios ^{3,*} and Fabrizio Ortu ^{1,*}

¹ School of Chemistry, University of Leicester, University Road, Leicester LE1 7RH, UK; mps28@leicester.ac.uk (M.P.S.); emily.spray@hotmail.co.uk (E.S.); ks42@leicester.ac.uk (K.S.); vanessa.timmermann@siigroup.com (V.M.T.)

² Department of Chemistry, The University of Manchester, Oxford Road, Manchester M13 9PL, UK; inigo.vitorica@manchester.ac.uk

³ Institute of Chemical Sciences, Heriot-Watt University, Edinburgh EH14 4AS, UK

* Correspondence: l.sotorrios@hw.ac.uk (L.S.); fabrizio.ortu@leicester.ac.uk (F.O.); Tel.: +44-(0)116-294-4670 (F.O.)

Abstract: Herein, we report the synthesis of a series of heteroleptic magnesium complexes stabilized with the scorpionate ligand tris(2-pyridylthio)methanide (Tptm). The compounds of the general formula [Mg(Tptm)(X)] (1-X; X = Cl, Br, I) were obtained via protonolysis reaction between the proligand and selected Grignard reagents. Attempts to isolate the potassium derivative K(Tptm) lead to decomposition of Tptm and formation of the alkene (C₅H₄N-S)₂C=C(C₅H₄N-S)₂, and this degradation was also modelled using DFT methods. Compound 1-I was treated with K(CH₂Ph), affording the degradation product [Mg(Bptm)₂] (2; Bptm = {CH(S-C₅NH₃)₂}⁻). We analyzed and quantified the steric properties of the Tptm ligand using the structural information of the compounds obtained in this study paired with buried volume calculations, also adding the structural data of HTptm and its CF₃-substituted congener (HTptm^{CF3}). These studies highlight the highly flexible nature of this ligand scaffold and its ability to stabilize various coordination motifs and geometries, which is a highly desirable feature in the design of novel organometallic reagents and catalysts.

Keywords: organometallic chemistry; alkaline earth; inorganic; scorpionate; ligand design; DFT; buried volume calculations



Citation: Stevens, M.P.; Spray, E.; Vitorica-Yrezabal, I.J.; Singh, K.; Timmermann, V.M.; Sotorrios, L.; Ortu, F. Structural Investigation of Magnesium Complexes Supported by a Thiopyridyl Scorpionate Ligand. *Molecules* **2022**, *27*, 4564. <https://doi.org/10.3390/molecules27144564>

Academic Editors: Vito Lippolis, Franco Bisceglie, Dubravka Matković-Čalogović, Carla Bazzicalupi, Serenella Medici, M.-H. Whangbo, Shigeyoshi Inoue and Andrea Bencini

Received: 23 June 2022

Accepted: 14 July 2022

Published: 18 July 2022

Publisher's Note: MDPI stays neutral with regard to jurisdictional claims in published maps and institutional affiliations.



Copyright: © 2022 by the authors. Licensee MDPI, Basel, Switzerland. This article is an open access article distributed under the terms and conditions of the Creative Commons Attribution (CC BY) license (<https://creativecommons.org/licenses/by/4.0/>).

1. Introduction

Bulky, multidentate ligands have found extensive use for the stabilization of alkaline earth (AE) metal complexes, owing to their ability to saturate the metal coordination sphere, preventing unwanted attacks from large donor groups [1–4]. Ligands of this type can be designed and tailored to offer one open face in the metal coordination sphere, which can be used for selective reactivity or further functionalization [5]. An example of the application of bulky, multidentate ligands in AE chemistry is the substituted tris(pyrazolyl)borate (Tp) architectures [6]; recently, the extremely bulky tris(3-*t*-Bu-5-Me-pyrazole)borate (Tp^{*t*Bu,Me}) ligand was used by Anwender and co-workers to stabilise the complex [Ca(Tp^{*t*Bu,Me})(Me)], which contains an unprecedented terminal Ca–Me bond. [7] This is a highly reactive functionality due to the large charge separation between the metal and carbon atom; in this case, the scorpionate Tp^{*t*Bu,Me} ligand is providing steric protection to the Ca–C bond [7], together with preventing dimerization and Schlenk equilibrium-type rearrangements [8].

Tp ligands are classic examples of scorpionate-type donors, which are capable of wrapping around the metal centre in a κ³-fashion. Scorpionate ligands can be further extended with the addition of a fourth coordination point which acts as an anchor. A good example of this approach is the tris([1-isopropylbenzamido-2-yl]-dimethylsilyl)methyl ligand, (Tism^{PriBenz}), which was utilized to form the terminal magnesium-methyl complex

[Mg(Tism^{PriBenz})(Me)] and can be converted into the parent hydride [Mg(Tism^{PriBenz})(H)] [9]. The latter complex has found extensive applications as a catalyst for hydroboration and hydrosilylation of styrene and carbodiimides [10].

Tris(2-pyridylthio)methanide, {CH(S-C₅NH₄)₃}[−] (Tptm), is another example of a scorpionate ligand, which was first used by Kinoshita and co-workers to prepare various first-row transition metal complexes [11–13]. In further work, the same authors reported the preparation of heteroleptic Zn complexes of formula [Zn(Tptm)(X)] (X = Cl, Br); these species were obtained by reacting HTptm with ZnX₂ (X = Cl, Br) in the presence of K₂CO₃ [14]. Parkin and co-workers subsequently reported a series of zinc complexes of general formula [Zn(Tptm)(X)] (X = Me, N(SiMe₃)₂), which were prepared via protonolysis from the corresponding homoleptic Zn bis-amide or bis-alkyl precursor; additionally, these functionalities can be exchanged to increase the reactivity of these complexes, by installing silyloxy or hydride functionalities [15]. An example of this is the reactivity of the heteroleptic zinc complex [Zn(Tptm){N(SiMe₃)₂}], which reacts readily with CO₂ to give isocyanate complex [Zn(Tptm)(NCO)]; its hydride congener [Zn(Tptm)(H)] also reacts with CO₂, affording formate species [Zn(Tptm)(O₂CH)] [15].

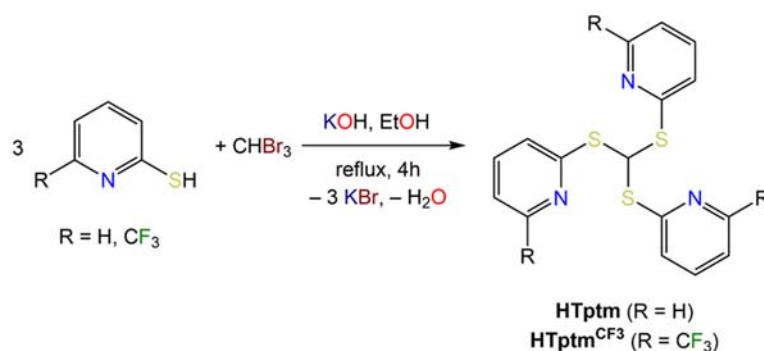
Owing to the similarities between Zn²⁺ and Mg²⁺ for their coordination chemistry (Zn²⁺ 0.74 Å, Mg²⁺ 0.72 Å) [16], we were interested in extending the use of Tptm to Mg with the goal of isolating new heteroleptic complexes and exploring their reactivity towards small molecules. Ligand design is a crucial aspect in the preparation of reactive organometallic species, and the work of Kinoshita and Parkin with Tptm-supported complexes shows that this ligand system offers a certain degree of flexibility which could be exploited for the preparation of various heteroleptic species [14,15]. In the Zn complexes reported by these authors, [Zn(Tptm)(X)] (X = H, Me, N(SiMe₃)₂, F, Cl, Br, OH, OSiMe₃, NCO), the Tptm ligand, switches between a κ³ and κ⁴ binding arrangement depending on the types of ligands bound to the metal centre [14,15,17,18]. We envisaged that a good starting point for our synthetic journey would be to prepare some model magnesium compounds and assess the coordination chemistry of the Tptm ligand. Whilst structural studies provide an excellent representation of coordination motifs, several other tools can be used to quantify the steric properties of the supporting ligands. The Tolman cone angle is probably the most famous parameter used for this purpose, and its scope and application have recently been revisited, as shown by Anwender's cone-angle calculations carried out on scorpionate ligands bound to magnesium [19]. Other tools have also found applications in coordination and organometallic chemistry, such as the solid angle G parameter and buried volume (%V_{bur}) [20–22]. The latter calculations have been used quite extensively over the last decade to quantify the amount of steric protection imparted by ligands, and they have entered routine use for ligand design [20,21]. Though initially developed for NHC ligands [23], these calculations have been applied extensively in Group 2 coordination chemistry, encompassing ligands with various binding modes, denticity, and steric features [24,25]. Therefore, we believed this tool could provide a quantitative assessment of the steric features of the Tptm ligand architecture in order to inform our ligand design strategy. Herein, we present the synthesis of a small family of heteroleptic magnesium halide complexes supported by Tptm, accompanied by a structural analysis based on the combination of single crystal XRD studies and %V_{bur} calculations.

2. Results

Synthesis and NMR Characterization

The proligand tris(2-pyridylthio)methane (HTptm) was synthesized following minor modifications of literature methods reported by Parkin and co-workers (Scheme 1) [15]. The preparation of HTptm was first reported by de Castro et al., who followed a slightly different methodology [26], though we could not reproduce their yields. It is also noteworthy that Kinoshita et al. used a different approach for the preparation of HTptm, which involved sonication of the reaction mixture and shorter reaction times. We were able to reproduce Parkin's methodology very reliably and adapted their methods for synthesizing

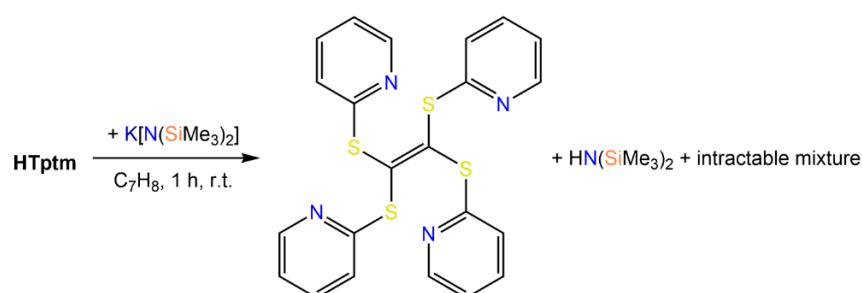
a more sterically demanding version of this architecture, comprising CF_3 substituents in the 6-position on the pyridyl arms, i.e., $\text{HC}[\text{S}\{\text{C}_5\text{H}_3\text{N}(\text{CF}_3)\text{-6}\}]_3$ ($\text{HTptm}^{\text{CF}_3}$). However, its synthesis proved to be significantly more challenging than that of HTptm ; our methodology affords $\text{HTptm}^{\text{CF}_3}$ in very poor yields (ca. 5%) therefore, it could only be made in small quantities sufficient for its full spectroscopic characterization.



Scheme 1. Synthesis of HTptm and $\text{HTptm}^{\text{CF}_3}$.

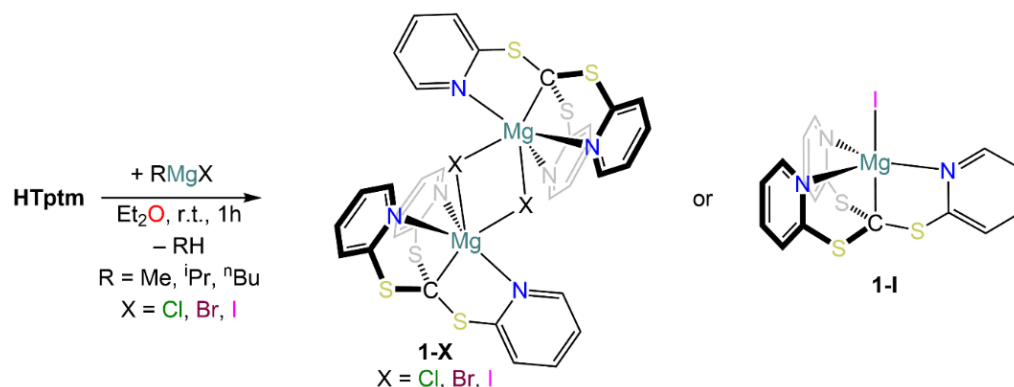
The ^1H NMR spectrum of $\text{HTptm}^{\text{CF}_3}$ displays a singlet at 8.11 corresponding to the CH methine proton (*c.f.* 7.90 ppm for HTptm), together with a triplet (7.68 ppm) and two doublets (7.40, 7.34 ppm) corresponding to protons H^b , H^a and H^c , respectively. In the $^{13}\text{C}\{^1\text{H}\}$ NMR spectrum of $\text{HTptm}^{\text{CF}_3}$, the quaternary CF_3 signal appears as a single large quartet owing to the strong $^1J_{\text{CF}}$ coupling (121.2 ppm, $^1J_{\text{CF}} = 273$ Hz), and coupling to ^{19}F is also observed in the signal of quaternary carbon C^a (148.1 ppm, $^2J_{\text{CF}} = 34.5$ Hz). Additionally, a slight broadening ($\nu_{\frac{1}{2}} = 7.0$ Hz) is observed for the $\text{C}^b\text{-H}$ signal (116.5 ppm), and the remaining $\text{C}^c\text{-H}$ and $\text{C}^d\text{-H}$ resonances are observed at 137.3 and 124.3 ppm, respectively. Finally, the $^{19}\text{F}\{^1\text{H}\}$ NMR spectrum of $\text{HTptm}^{\text{CF}_3}$ shows only one signal at 68.65 ppm, indicative of a single fluorine environment in solution.

Initially, we set out to prepare alkali metal salts of the Tptm ligand to be employed in salt elimination reactions. Parkin and co-workers reported a lithium derivative $\text{Li}(\text{Tptm})$ obtained from the reaction of HTptm with organolithium reagents [27]. We decided to attempt the preparation of the potassium analogue $\text{K}(\text{Tptm})$ from the reaction of $\text{K}[\text{N}(\text{SiMe}_3)_2]$ with HTptm in toluene (Scheme 2). DFT calculations suggest that this process, which also forms the free amine $\text{HN}(\text{SiMe}_3)_2$, is exergonic by 9.0 kcal/mol. However, the target compound decomposes readily to give the alkene $(\text{C}_5\text{H}_4\text{N-S})_2\text{C}=\text{C}(\text{C}_5\text{H}_4\text{N-S})_2$ and other by-products which could not be unequivocally identified. The detachment of a pyridyl arm from the Tptm scaffold has been previously observed by Kinoshita and co-workers when HTptm was reacted with FeI_2 in the presence of Et_3N and subsequent treatment with AgPF_6 , leading to an equilibrium between the carbene complex $[\text{Fe}\{\text{C}(\text{S-C}_5\text{H}_4\text{N})_2\}(\text{C}_5\text{H}_4\text{N-S})(\text{I})]$ and $[\text{Fe}(\text{Tptm})(\text{CH}_3\text{CN})_2][\text{PF}_6]$ [28]. However, the formation of $(\text{C}_5\text{H}_4\text{N-S})_2\text{C}=\text{C}(\text{C}_5\text{H}_4\text{N-S})_2$ has not been previously reported. DFT calculations showed the formation of this decomposition product along with one equivalent of $\text{K}(\text{C}_5\text{H}_4\text{N-S})$ is favoured by 14.2 kcal/mol, with the decomposition reaction balanced assuming the formation of $\text{K}(\text{C}_5\text{H}_4\text{N-S})$.



Scheme 2. Reactivity of $\text{K}[\text{N}(\text{SiMe}_3)_2]$ with HTptm and formation of $(\text{C}_5\text{H}_4\text{N-S})_2\text{C}=\text{C}(\text{C}_5\text{H}_4\text{N-S})_2$.

We then decided to use a different approach for the synthesis of magnesium complexes involving a single-step protonolysis reaction. Protonolysis methodologies involving Grignard reagents are a common synthetic strategy in AE coordination and organometallic chemistry [29]. Hence, HTptm was reacted with selected Grignard reagents (i.e., $^i\text{PrMgCl}$, MeMgBr and MeMgI) in diethyl ether at room temperature (Scheme 3), producing the target complexes $[\text{Mg}(\text{Tptm})(\text{Cl})]$ (**1-Cl**), $[\text{Mg}(\text{Tptm})(\text{Br})]$ (**1-Br**) and $[\text{Mg}(\text{Tptm})(\text{I})]$ (**1-I**) with the concomitant formation of propane or methane. In all cases, the target compounds were obtained in excellent yields (>90%), and their formulations were confirmed via elemental analyses.



Scheme 3. Synthesis of **1-Cl**, **1-Br** and **1-I**.

The ^1H NMR spectra of **1-Cl**, **1-Br** and **1-I** bear many similarities and clearly show the three pyridyl protons in the aromatic region (Table 1). Only one set of signals is present in each case, thus hinting at the presence of a C_3 -symmetrical arrangement around the metal centre in solution for all complexes. Interestingly, there are some significant changes in the chemical shift of the pyridyl proton signals across the three compounds, though this behaviour does not appear to follow a specific trend (Table 1). For instance, proton H^a (Figure 1) resonates at 9.61 ppm for **1-Cl**, and the same signal is more shielded in **1-Br** (8.22 ppm) and more deshielded in **1-I** (9.88 ppm). However, the chemical shifts of the relative C-H signals in the $^{13}\text{C}\{^1\text{H}\}$ NMR spectra show very few variations across all these species. Nonetheless, the resonance of the methanide carbon is approximately the same in **1-Cl** and **1-Br** (15.0 and 15.1 ppm respectively), whilst it is significantly shifted in **1-I** (33.0 ppm); these signals are particularly difficult to detect and have not been reported before for analogous species such as $[\text{Zn}(\text{Tptm})\{\text{N}(\text{SiMe}_3)_2\}]$ [15].

Table 1. ^1H NMR shifts of **1-X**.

Compound	H^a	$\text{H}^{c,d}$	H^b
1-Cl	9.61	6.45–6.48	6.19
1-Br	8.22	6.18, 6.52	5.99
1-I	9.88	6.15–6.19	6.42

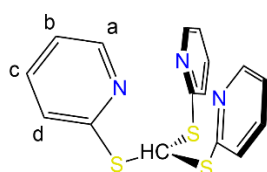
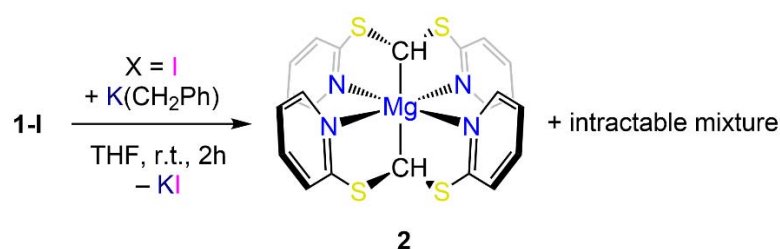


Figure 1. Atom labelling of HTptm.

Halide functionalities can be replaced via simple salt elimination protocols with Group 1 reagents. With the idea of using this strategy to obtain a heteroleptic alkyl derivative of formula $[\text{Mg}(\text{Tptm})(\text{CH}_2\text{Ph})]$, **1-I** was reacted with one equivalent of $\text{K}(\text{CH}_2\text{Ph})$ in

THF at room temperature (Scheme 3). Instead of isolating the target complex, a few crystals of $[\text{Mg}(\text{Bptm})_2]$ (**2**; $\text{Bptm} = \{\text{CH}(\text{S}-\text{C}_5\text{NH}_3)_2\}^-$) were obtained together with an intractable mixture of products (Scheme 4). The reasons for the formation of **2** are unclear; initially, the reaction produces a white precipitate which suggests that a salt elimination reaction is taking place, which generates KI. Therefore, we postulate that **2** is likely formed from the decomposition of the target complex $[\text{Mg}(\text{Tptm})(\text{CH}_2\text{Ph})]$, rather than from undesired reactivity of $\text{K}(\text{CH}_2\text{Ph})$ with **1-I**. The ^1H NMR spectrum of **2** displays one set of four proton signals in the aromatic region ($\delta_{\text{H}} = 5.98, 6.18, 6.52$ and 8.32 ppm), indicative of the presence of a highly symmetric species in solution; accordingly, one single proton environment is observed for the hydrogen atom bound to the carbon donor on the two Bptm ligands ($\delta_{\text{H}} = 5.15$ ppm). The $^{13}\text{C}\{^1\text{H}\}$ NMR spectrum also confirms the highly symmetrical nature of **2** in solution, showing a single environment for each aromatic carbon of Bptm ($\delta_{\text{C}} = 117.9, 121.6, 135.9, 147.2$ and 166.5). Additionally, we were able to identify a signal resonating at 20.0 ppm, which can be assigned to the methanide carbon bound to Mg.



Scheme 4. Reactivity of **1-I** with $\text{K}(\text{CH}_2\text{Ph})$ and isolation of **2**.

3. Structural Characterization and Buried Volume Calculations

XRD studies were carried out on single crystals of $\text{HTptm}^{\text{CF}_3}$ grown from an ethanol solution at room temperature. $\text{HTptm}^{\text{CF}_3}$ crystallizes in the $P2_1/c$ space group, and its molecular structure clearly shows that the pseudo- C_3 symmetric conformation of HTptm is not possible with this species (Figure 2). Instead, one of the thiopyridyl arms sits below the plane of the sulfur atoms relative to the other two arms of the ligand. The H-C-S-C torsional angle of the thiopyridyl arm relative to the methanide C-H bond is $29.3(3)^\circ$, relative to 43.6° for HTptm, indicating that there is less steric clash about the central methanide in the substituted ligand relative to the parent, albeit with a considerable conformational difference.

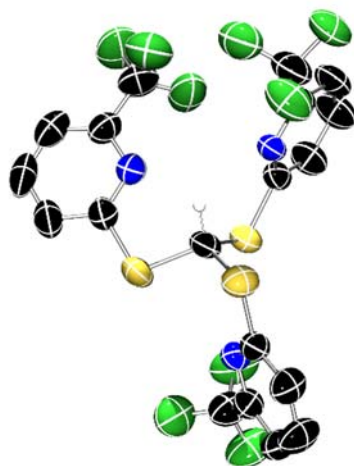


Figure 2. X-ray crystal structure of $\text{HTptm}^{\text{CF}_3}$. Ellipsoids are set at 50% probability level, and selected hydrogen atoms and disordered fluorine atoms have been excluded for clarity. C: black; N: blue; S: yellow; F: green.

Single crystals suitable for XRD studies were obtained for **1-Cl**, **1-Br** and **1-I** (Figure 3), which confirmed the proposed connectivity in all cases. All three halide complexes crystallize as dimers, $[\{\text{Mg}(\text{Tptm})(\mu\text{-X})\}_2]$, in which the halides bridge between two 6-coordinate Mg centres. In contrast to **1-Br** and **1-Cl**, the crystal structure of **1-I** also contains a monomeric molecule of **1-I** in addition to the dimer (Figure 4). This has a very high degree of disorder, and so whilst the connectivity is clear-cut, it is difficult to make any statistically valid comparisons or comments on bond distances and angles. However, it would appear that in the absence of a sixth coordination point, the magnesium adopts a distorted trigonal bipyramidal geometry. The Mg–C distances in **1-X** [Cl: 2.427(11); Br: 2.231(11); I: 2.231(10) Å] are similar to the analogous Mg–C bond in **2** [2.303(4) Å] and quite close to that observed for the related $[\text{Zn}(\text{Tptm})(\text{Cl})]$ complex prepared by Kinoshita and co-workers [2.19(2), 2.213(6) Å] [14] and $[\text{Mg}(\text{Tptm})\{\text{N}(\text{SiMe}_3)_2\}]$ [2.303(4) Å] [30]. The Mg–N_{py} bond distances [Cl: 2.186(11)–2.204(10); Br: 2.155(9)–2.219(9); I: 2.177(8)–2.182(8) Å] also fall within the range observed for analogous complexes [2.203(2)–2.305(2) Å] [30,31]. In all three **1-X** complexes, the geometry around the metal atom can be described as *mer-mer* with the three nitrogen atoms forming one meridional plane and the two halide atoms and methanide carbon forming the other.

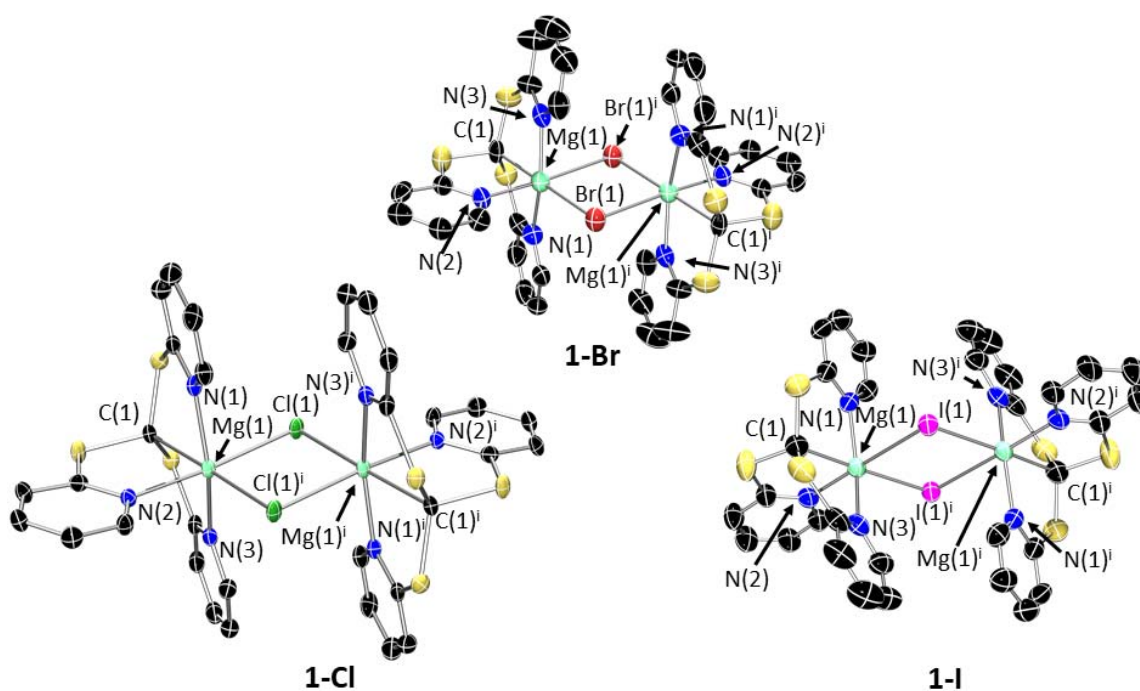


Figure 3. X-ray crystal structures of **1-X** (X = Cl, Br, I). Ellipsoids are set at 50% probability level, and hydrogen atoms and lattice solvent molecules have been excluded for clarity. The figures have been reproduced as dimers to fully illustrate the geometry. C: black; N: blue; S: yellow; Mg: aquamarine; Cl: green; Br: brown; I: purple. **1-Cl**: The asymmetric unit contains one monomer and half a molecule of benzene. Symmetry operation used to generate equivalent atoms: $i = -x, 0.5 + y, 0.5 - z$. Selected bond lengths (Å) and angles (°): Mg(1)–C(1) 2.427(11), Mg(1)–N(1) 2.186(11), Mg(1)–N(2) 2.204(10), Mg(1)–N(3) 2.193(11), Mg(1)–Cl(1) 2.427(5), N(1)–Mg(1)–N(2) 87.1(4), N(2)–Mg(1)–N(3) 94.1(4), C(1)–Mg(1)–Cl(1) 178.9(4). **1-Br**: The asymmetric unit contains two monomers. Symmetry operation used to generate equivalent atoms: $i = 1 - x, 2 - y, 1 - z$. Selected bond lengths (Å) and angles (°): Mg(1)–C(1) 2.231(11), Mg(1)–N(1) 2.219(9), Mg(1)–N(2) 2.155(9), Mg(1)–N(3) 2.182(9), Mg(1)–Br(1) 2.821(4), N(1)–Mg(1)–N(2) 92.9(3), N(2)–Mg(1)–N(3) 92.1(3), C(1)–Mg(1)–Br(1) 94.2(3). **1-I**: Symmetry operation used to generate equivalent atoms: $i = 2 - x, 1 - y, 1 - z$. Selected bond lengths (Å) and angles (°): Mg(1)–C(1) 2.231(10), Mg(1)–N(1) 2.182(8), Mg(1)–N(2) 2.177(8), Mg(1)–N(3) 2.177(8), Mg(1)–I(1) 2.855(3), N(1)–Mg(1)–N(2) 95.8(3), N(2)–Mg(1)–N(3) 93.5(3), C(1)–Mg(1)–I(1) 177.4(3).

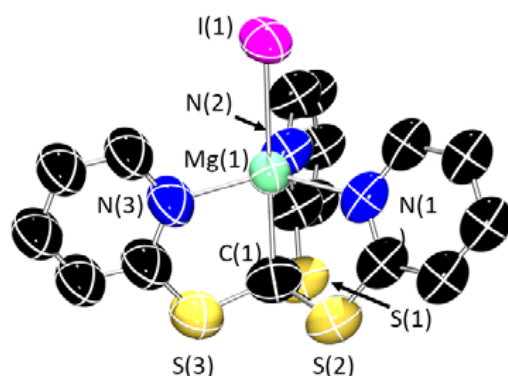


Figure 4. X-ray crystal structure of monomeric **1-I**. Ellipsoids are set at 50% probability level, and hydrogen atoms have been excluded for clarity. C: black; N: blue; S: yellow; Mg: aquamarine; I: purple.

In one instance, we were able to obtain the molecular structure of the THF adduct $[\text{Mg}(\text{Tptm})(\text{I})(\text{THF})]$ (**1-I**·THF); **1-I**·THF also adopts an octahedral geometry about magnesium, featuring the iodide ligand in an apical position in trans to the methanide carbon (Figure 5), analogously to monomeric **1-I**. The Mg–C distance [2.265(15) Å] is slightly longer than in unsolvated **1-I**, but still within the range of the values above. The Mg–N_{py} bond distance [2.213(13)–2.232(12) Å] is also slightly longer than the dimeric form but within the typical range [30,31].

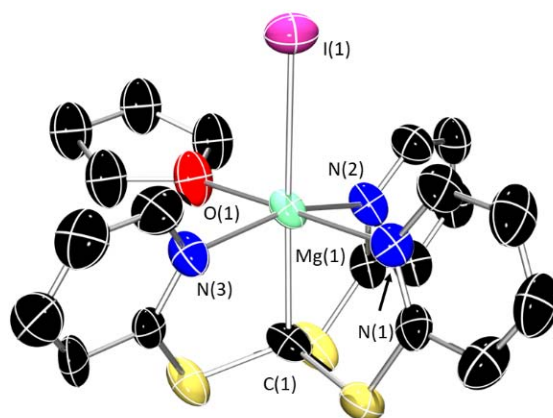


Figure 5. X-ray crystal structure of **1-I**·THF. Ellipsoids are set at 50% probability level, and hydrogen atoms and disordered THF have been excluded for clarity. C: black; N: blue; S: yellow; Mg: aquamarine; I: purple; O: red. Selected bond lengths (Å) and angles (°): Mg(1)–C(1) 2.265(15), Mg(1)–N(1) 2.232(12), Mg(1)–N(2) 2.224(13), Mg(1)–N(3) 2.213(13), Mg(1)–I(1) 2.886(5), N(1)–Mg(1)–N(3) 90.8(6), N(1)–Mg(1)–N(2) 93.3(6), C(1)–Mg(1)–I(1) 177.8(4).

Compound **2** crystallizes in the triclinic $P\bar{1}$ and features Mg in a 6-coordinate environment in what could be deemed as a distorted octahedral geometry (Figure 6). The complex is very symmetrical, with a perfect 180° angle between the two methanide carbon atoms, C(1) and C(1)ⁱ, and the metal centre. The four pyridyl nitrogen atoms complete the coordination sphere of magnesium by coordinating equatorially and with angles close to an ideal square planar arrangement [N–Mg–N 97.74(13)° and 87.26(13)°]. The Mg–C [2.235(5) Å] and Mg–N distances [2.201(4) Å and 2.226(3) Å] are consistent with those observed in **1-X**.

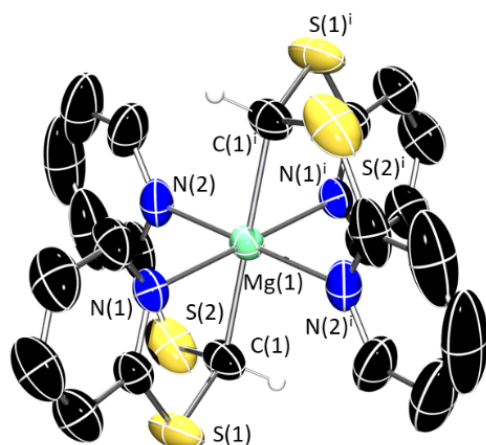


Figure 6. X-ray crystal structure of **2**. Ellipsoids are set at 50% probability level, and the benzene lattice solvent and selected hydrogen atoms have been excluded for clarity. The figure has been reproduced as a dimer to fully illustrate the geometry. Symmetry operation used to generate equivalent atoms: $i = -x, -1 - y, -1 - z$. C: black; N: blue; S: yellow; Mg: aquamarine. Selected bond lengths (Å) and angles (°): Mg(1)–C(1) 2.236(5), Mg(1)–N(1) 2.201(5), Mg(1)–N(2) 2.226(5), N(1)–Mg(1)–N(2) 92.7(2), C(1)–Mg(1)–C(1)ⁱ 180.0(6), N(1)–Mg(1)–N(1)ⁱ 180.0(5), N(2)–Mg(1)–N(2)ⁱ 180.0(6), N(1)–Mg(1)–C(1) 82.6(2), N(2)–Mg(1)–C(1) 82.4(2).

Working from crystal structures, the percentage buried volume, $\%V_{\text{bur}}$, was calculated using SambVca [20,21]. It was determined that the proligand HTptm, if coordinated to a metal without any change to the geometry, would occupy 66.7% of the coordination sphere of that metal (coordination axis, viewpoint and “top-down” steric maps are given in Figures 7–9). In contrast, HTptm^{CF₃} was found to have a significantly higher $\%V_{\text{bur}}$ of 75.7%; this is despite its arrangement in the solid state with one of the pyridyl arms flipped below the steric pocket. Buried volumes were also calculated for the Tptm ligand in the series of heteroleptic magnesium complexes **1-X** (Table 2). It was found the $\%V_{\text{bur}}$ of Tptm does not vary across the series of heteroleptic halide dimers (65.7%) and is close to the volume occupied by Tptm in the monomeric THF adduct **1-I·THF** (64.3%). However, $\%V_{\text{bur}}$ increases significantly in the case of monomeric **1-I** (75.3%), where the arrangement of Tptm forces the Mg centre in a 5-coordinate geometry (trigonal bipyramid) compared to a more open conformation in the 6-coordinate bridged halide dimers. For completeness, we also performed $\%V_{\text{bur}}$ calculations of Bptm by extracting coordinates from the molecular structure of **2** (Figure 10). As expected, Bptm displays a significantly smaller $\%V_{\text{bur}}$ (48.2%) compared to Tptm in any of the complexes reported in this work.

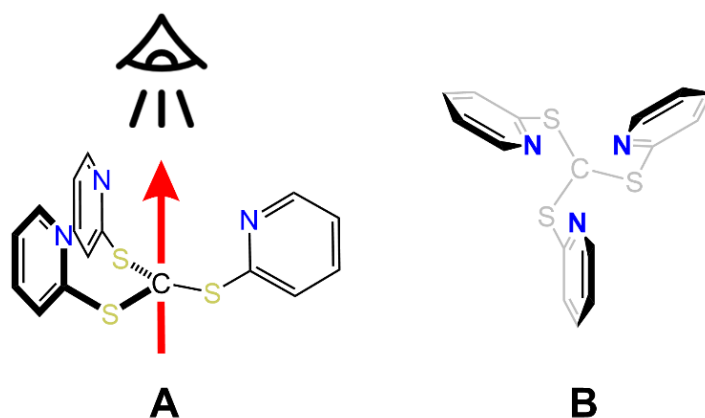


Figure 7. Coordination axis (A) and viewpoint (A,B) employed for the $\%V_{\text{bur}}$ calculation of Tptm and representation of associated steric maps.

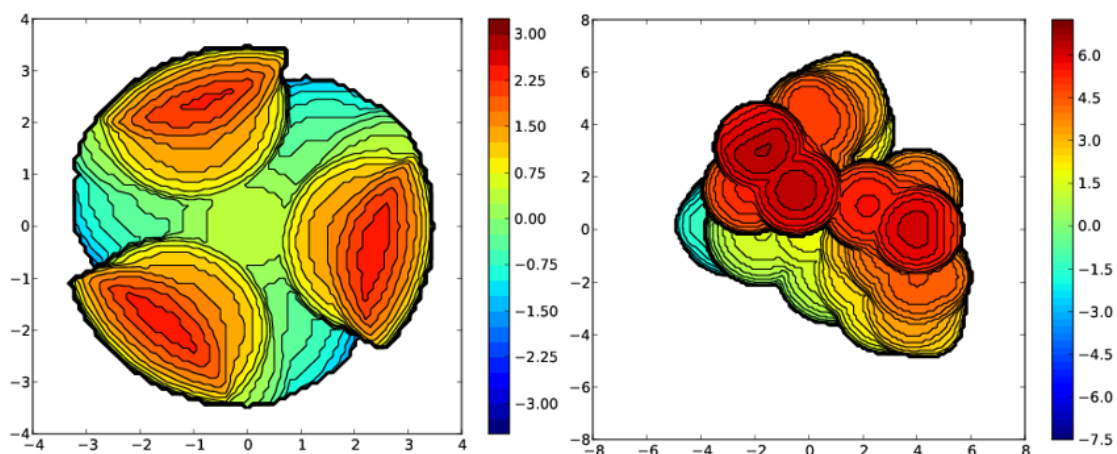


Figure 8. Steric maps of HTptm (left) generated with a coordination sphere of 3.5 Å and HTptm^{CF3} (right), generated with a coordination sphere of 7.5 Å to give a more representative image.

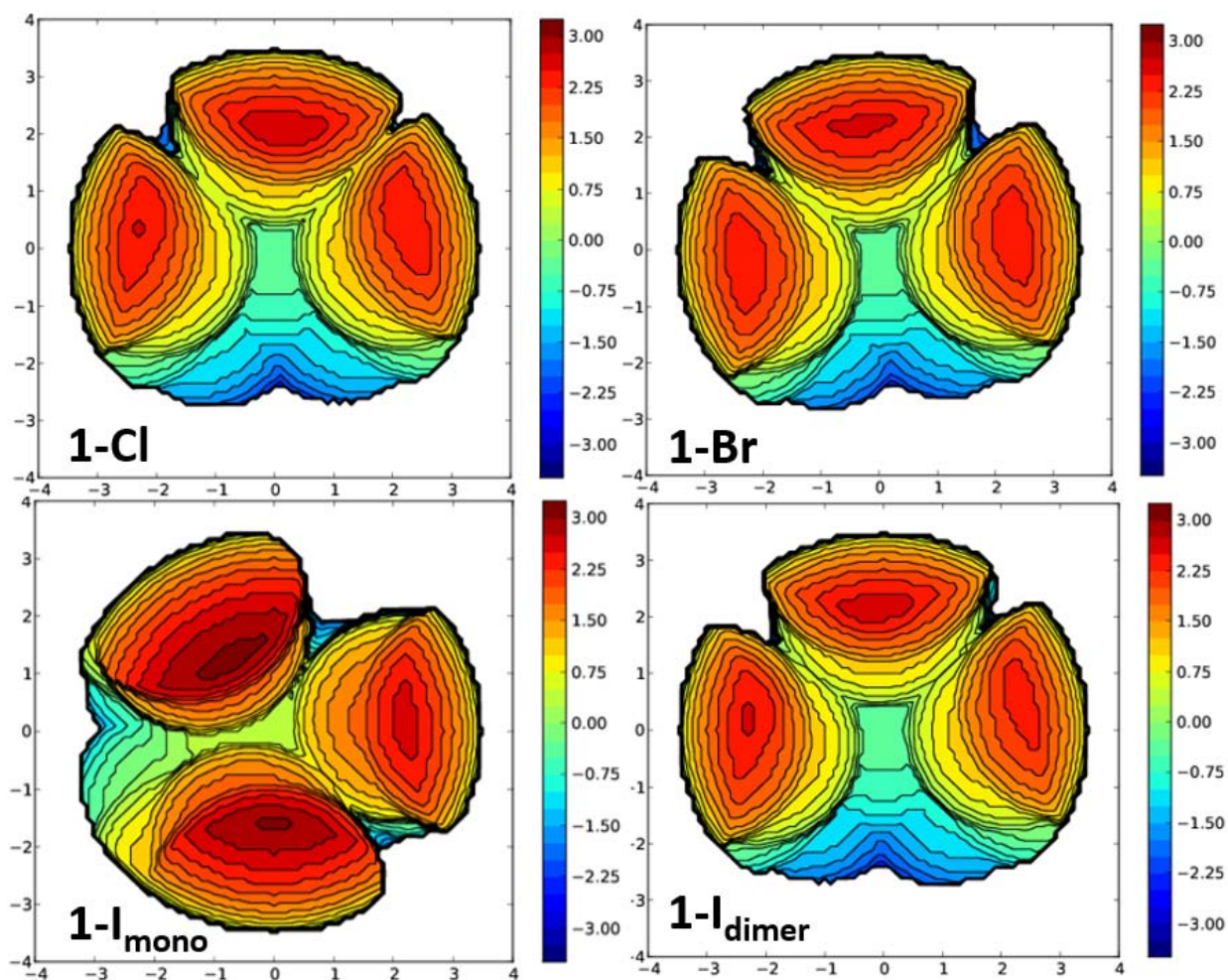


Figure 9. Steric map of the Tptm in 1-X (dimeric, clockwise from top left: X = Cl, Br, I), and monomeric 1-I (bottom left). Generated from buried volume calculations with a coordination sphere of 3.5 Å.

Table 2. Buried volume calculations using crystallographic coordinates of HTptm and HTptm^{CF3}, along with complexes of Tptm and **2**. **1-Br** and **1-Cl** are isostructural.

Compound	%V _{bur}
HTptm	66.7
HTptm ^{CF3}	75.7
1-Cl/Br	65.7
1-I (dimeric)	65.7
1-I (monomeric)	75.3
1-I ·THF	64.3
2	48.2

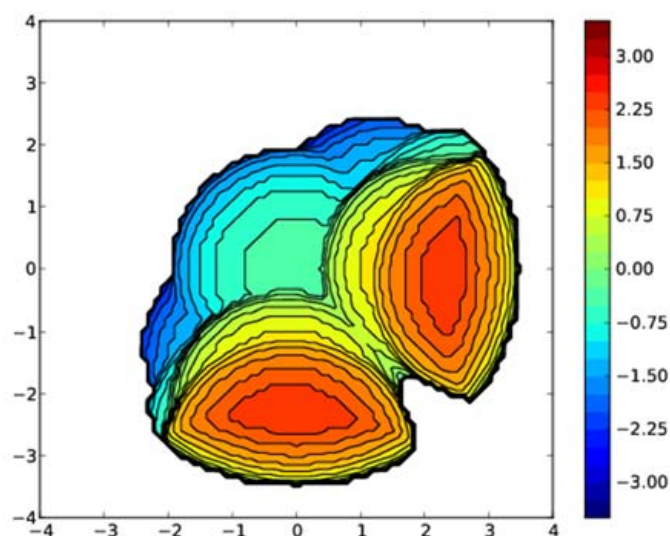


Figure 10. Steric map of the Bptm ligand in **2**. Generated from buried volume calculations with a coordination sphere of 3.5 Å.

4. Discussion

Analysis of solid state structures combined with %V_{bur} calculations highlights the very flexible nature of the Tptm ligand. When Tptm binds a magnesium centre, its κ^4 coordination mode affords two main conformations: ‘open’ and ‘closed’. In both conformations, the CS₃ base of the tripodal ligand maintains a trigonal pyramidal geometry, whilst the pyridyl arms twist to form either an equatorial coordination arrangement around the Mg centre that is either *pseudo*-trigonal planar (‘closed’) or T-shaped (‘open’) (N∠N changes from 104.7(7)–132(2)° to 93.5(3)–96.1(3)°). As a result, complexes in the ‘open’ conformation feature a 6-coordinate magnesium centre, which is the coordination motif observed for **1-I**·THF and halide bridged dimers **1-X**. Conversely, in the ‘closed’ conformation (such as for monomeric **1-I** and [Mg(Tptm){N(SiMe₃)₂}] [24]), the CS₃ base has a *pseudo* C₃ symmetry that results in a better equatorial coordination saturation of the metal by the ligand pyridyl arms. Further flexibility still was observed in the analogous zinc complexes of general formula [Zn(Tptm)(X)] (X = H, Me, N(SiMe₃)₂) reported by Parkin and co-workers, wherein Tptm acts as a k^3 donor, with one of the pyridyl pendant arms flipped below the steric pocket [15]. This is strongly reminiscent of the crystal structure of HTptm^{CF3}. Therefore, we expect that Tptm^{CF3} will act exclusively as a k^3 donor owing to its high steric demands.

5. Conclusions

In summary, we reported the synthesis and structural authentication of a series of heteroleptic magnesium-halide complexes (**1-X**; X = Cl, Br, I) supported by the scorpionate Tptm ligand, obtained via protonolysis reactivity between the proligand and selected Grignard reagents. Attempts to prepare the potassium derivative K(Tptm) led to facile

decomposition of the ligand and identification of the alkene $(C_5H_4N-S)_2C=C(C_5H_4N-S)_2$; the energetic profile of this degradation pathway was also further analysed via DFT calculations which highlighted the exergonic nature of this process. Additionally, attempts to functionalise **1-I** with $K(CH_2Ph)$ also led to decomposition of Tptm and formation of **2**. Finally, we utilized the structural information obtained on all these complexes to assess the steric properties of Tptm and quantified these using buried volume calculations. Our studies highlight the high flexibility of the Tptm scaffold, which derives from the flexibility of its CS_3 base and the ability of the pyridyl sidearms to twist into different conformations. As such, Tptm can accommodate different coordination environments and geometries, including different ancillary ligands. This flexibility is a highly desirable feature in the design of new reagents and catalysts, and this study will inform future ligand design to stabilise magnesium complexes with precise structure-function relationships.

6. Materials and Methods

6.1. General Methods

THF, Et_2O , toluene and hexane were passed through columns containing molecular sieves, then stored over molecular sieves (THF) or over a potassium mirror (Et_2O , hexane, toluene) and thoroughly degassed prior to use. Anhydrous benzene was purchased from Sigma Aldrich, stored over a potassium mirror and thoroughly degassed prior to use. For NMR spectroscopy, C_6D_6 and C_4D_8O were dried by refluxing over K, $CDCl_3$ was dried by refluxing over CaH_2 ; NMR solvents were then vacuum transferred and degassed by three freeze-pump-thaw cycles before use. NMR spectra were recorded on either a Bruker AVIII HD 400 or Bruker AVIII 500 spectrometer operating at 400.07/500.13 (1H), 100.60/125.78 ($^{13}C\{^1H\}$), 376.46 ($^{19}F\{^1H\}$) MHz. NMR spectra were recorded at 298 K unless otherwise stated and were referenced to residual solvent signals in the case of 1H and $^{13}C\{^1H\}$ experiments. FTIR spectra were recorded on a Bruker Alpha II spectrometer with a Platinum-ATR module. Elemental microanalyses were carried out by Elemental Microanalysis Ltd. Lawson's reagent, 6-trifluoromethyl-2-pyridone, 2-mercaptopyridine, potassium hydroxide, bromoform, isopropylmagnesium chloride, methylmagnesium bromide, and methylmagnesium iodide were used as received. HTptm [25], 2-mercapto-6-trifluoromethylpyridine [32], and benzyl potassium [33] were prepared according to literature procedures.

6.2. Synthesis

HTptm^{CF3}: A solution of potassium hydroxide (2.313 g, 41.23 mmol) and 2-mercapto-6-trifluoromethylpyridine (4.751 g, 26.52 mmol) in ethanol (200 mL) was treated in a dropwise manner with bromoform (0.8 mL, 8.89 mmol) dissolved in ethanol (50 mL), then refluxed for 4 h. The solution was allowed to cool to room temperature and filtered. The solvent was removed in vacuo and the resultant residue was extracted into benzene, then passed through a silica plug. The solvent was removed in vacuo once more, and the resultant crude product recrystallized from ethanol. Crystals were isolated via decantation and washed with cold ethanol to give pure HTptm^{CF3} (0.250 g, 0.5 mmol, 5.2%) as large colourless crystals.

1H NMR (400 MHz, 298 K, $CDCl_3$): δ_H (ppm) = 7.34 (3H, d, $^3J_{HH}$ = 8.1 Hz, $C_5H_3N-CH^c$), 7.40 (3H, d, $^3J_{HH}$ = 7.6 Hz, $C_5H_3N-CH^a$), 7.68 (3H, t, $^3J_{HH}$ = 7.9 Hz, $C_5H_3N-CH^b$), 8.11 (1H, s, S_3CH^d) ppm. $^{13}C\{^1H\}$ NMR (100 MHz, 298 K, $CDCl_3$): δ_C (ppm) = 48.9 (s, S_3C^fH), 116.6 (br s, fwhm = 7.0 Hz, $C_5H_3N-C^bH$), 121.2 (q, $^1J_{CF}$ = 274 Hz, C^gF_3), 124.3 ($C_5H_3N-C^dH$), 137.3 ($C_5H_3N-C^cH$), 148.1 (q, $^2J_{CF}$ = 35.8 Hz, $C_5H_3N-C^aCF_3$), 158.7 ($C_5H_3N-C^fS$). $^{19}F\{^1H\}$ NMR (376 MHz, 298 K $CDCl_3$): δ_F (ppm) = -68.65 (9F, s, CF_3). Anal. calcd. for $C_{19}H_{10}F_9N_3S_3$: C, 41.68%; H, 1.84%; N, 7.68%. Found: C, 41.63%; H, 1.79%; N, 7.64%. FTIR: $\tilde{\nu}$ (cm^{-1}) = 2908, 1589, 1564, 1440, 1414, 1335, 1255, 1130, 1103, 988, 825, 799, 765, 737, 715, 672, 646, 517, 471.

General method for the synthesis of $[Mg(Tptm)(X)]$ (1-X; X = Cl, Br, I): Under an atmosphere of dry argon, tris(2-mercaptopyridyl)methane (HTptm, 0.686 g, 2.0 mmol) was weighed into a flamed Schlenk flask, and diethyl ether was added (40 mL) with stirring

to dissolve the reagent. A solution in Et₂O or THF of the corresponding Grignard reagent (2.0 mmol) was then added, and after stirring for 1 h at room temperature, the solution was filtered. The precipitate was dried to yield pale yellow powder. This was recrystallized from boiling toluene (X = Br, I) or benzene (X = Cl).

1-Cl: From ⁱPrMgCl (1.0 mL, 2.0 mmol, 2.0 M in THF). Yield: 0.787 g (98%). ¹H NMR (400 MHz, 298 K, C₆D₆): δ_H (ppm) = 6.19 (3H, m, C₅H₃N-CH^b), 6.47 (6H, m, C₅H₃N-CH^c and C₅H₃N-CH^d), 9.61 (3H, d, ³J_{HH} = 5.6 Hz, C₅H₃N-CH^a). ¹³C{¹H} NMR (125 MHz, 298 K, C₄D₈O): δ_C (ppm) = 15.0 (MgC), 118.7 (C₅H₃N-C^bH), 120.0 (C₅H₃N-C^cH), 137.9 (C₅H₃N-C^dH), 150.7 (C₅H₃N-C^aH), 165.3 (C₅H₃N-C^eH). Anal. calcd. for C₃₂H₂₄Cl₂Mg₂N₆S₆·C₄H₈O: C, 49.27%; H, 3.79%; N, 9.58%. Found: C, 49.74%; H, 3.99%; N, 9.20%. FTIR: $\tilde{\nu}$ (cm⁻¹) = 2918, 2852, 1585, 1554, 1456, 1413, 1283, 1131, 1045, 1003, 755, 720, 638, 586, 486, 412.

1-Br: From MeMgBr (0.238 g, 2.00 mmol, dissolved in Et₂O). Yield: 0.805 g (90%). ¹H NMR (400 MHz, 298 K, C₆D₆): δ_H (ppm) = 6.41 (3H, t, ³J_{HH} = 6.4 Hz, C₅H₃N-CH^b), 7.25 (3H, d, ³J_{HH} = 7.9 Hz, C₅H₃N-CH^d), 7.35 (3H, d, ³J_{HH} = 8.0 Hz, C₅H₃N-CH^c), 8.22 (3H, d, ³J_{HH} = 4.3 Hz, C₅H₃N-CH^a). ¹³C{¹H} NMR (125 MHz, 298 K, C₄D₈O): δ_C (ppm) = 15.1 (MgC), 118.7 (C₅H₃N-C^bH), 120.2 (C₅H₃N-C^cH), 138.1 (C₅H₃N-C^dH), 151.3 (C₅H₃N-C^aH), 180.7 (C₅H₃N-C^eH). Anal. calcd. for C₃₂H₂₄Br₂Mg₂N₆S₆·C₄H₁₀O: C, 44.69%; H, 3.54%; N, 8.69%. Found: C, 44.48%; H, 3.27%; N, 8.46%. FTIR: $\tilde{\nu}$ (cm⁻¹) = 3062, 2969, 2582, 1587, 1555, 1456, 1415, 1283, 1155, 1131, 1091, 1046, 1003, 766, 756, 721, 638, 592, 485, 411.

1-I: From MeMgI (0.332 g, 2.00 mmol, dissolved in Et₂O). Yield: 938 mg (95%). ¹H NMR (400 MHz, 298 K, C₆D₆): δ_H (ppm) = 6.16 (3H, m, C₅H₃N-CH^b), 6.42 (6H, m, C₅H₃N-CH^c and C₅H₃N-CH^d), 9.88 (3H, d, ³J_{HH} = 5.7 Hz, C₅H₃N-CH^a). ¹³C{¹H} NMR (100 MHz, 298 K, C₆D₆): δ_C (ppm) = 33.0 (MgC), 118.6 (C₅H₃N-C^bH), 120.4 (C₅H₃N-C^cH), 138.0 (C₅H₃N-C^dH), 151.8 (C₅H₃N-C^aH), 164.8 (C₅H₃N-C^eH). Anal. calcd. for C₃₂H₂₅I₂Mg₂N₆S₆·0.5(C₄H₁₀O): C, 39.82%; H, 2.95%; N, 8.20%. Found: C, 39.50%; H, 2.65%; N, 8.04%. FTIR: $\tilde{\nu}$ (cm⁻¹) = 3066, 3009, 2972, 2865, 1588, 1555, 1458, 1413, 1283, 1131, 1091, 1046, 1002, 960, 879, 768, 756, 723, 640, 597, 484, 410.

2: To a flamed Schlenk flask was added 1-I (0.493 g, 1.00 mmol), benzyl potassium (0.130 g, 1.00 mmol), and tetrahydrofuran (40 mL). The reaction mixture was stirred overnight at room temperature, yielding a red solution. The precipitate was filtered off, and the solvent was removed from the filtrate in vacuo. The residue was extracted with benzene, and the solvent was removed in vacuo. The crude product was recrystallized from toluene, affording a small crop of crystals of 2 (ca. 20 mg). ¹H NMR (400 MHz, 298 K, C₆D₆): δ_H (ppm) = 5.15 (2H, s, MgCH), 5.98 (4H, t, ³J_{HH} = 6.3 Hz, C₅H₃N-CH^b), 6.18 (4H, t, ³J_{HH} = 7.7 Hz, HC(C₅H₃N-CH^d), 6.52 (4H, d, ³J_{HH} = 8.2 Hz, C₅H₃N-CH^c), 8.32 (4H, d, ³J_{HH} = 5.1 Hz, C₅H₃N-CH^a). ¹³C{¹H} NMR (100 MHz, 298 K, C₆D₆): δ_C (ppm) = 20.0 (MgCH), 117.9 (C₅H₃N-C^bH), 121.6 (C₅H₃N-C^dH), 135.9 (C₅H₃N-C^cH), 147.2 (C₅H₃N-C^aH), 166.5 (C₅H₃N-C^eH).

(C₅H₄N-S)₂C=C(C₅H₄N-S)₂: Tris(2-mercaptopyridyl)methane (HTptm, 686 mg, 2.0 mmol) and potassium bis(trimethylsilyl)amide (378 mg, 2.0 mmol) were weighed into a flamed Schlenk flask, and toluene added (50 mL) with stirring to dissolve the reagents. After stirring for 1 h, a chestnut precipitate formed, and the reaction mixture was transferred to the freezer overnight. The precipitate was filtered off, and recrystallization from toluene afforded a small crop of crystals of (C₅H₄N-S)₂C=C(C₅H₄N-S)₂ (ca. 10 mg), sufficient only for XRD characterisation.

6.3. Computational Methods

DFT geometry optimizations were run with Gaussian 16 (Revision A.03) [34] using the BP86 functional [35,36]. Si, S and K centres were described with the Stuttgart RECPs and associated basis sets [37], and 6-31G** basis sets were used for all other atoms [38,39]. A set of *d*-orbital polarization functions was also added to Si ($\zeta^d = 0.284$), S ($\zeta^d = 0.503$) and K ($\zeta^d = 1.000$) [40]. Stationary points were characterized by analytical frequency calculations that also provided the thermochemical corrections for the final free energies

reported in the text. Electronic energies were re-computed using the triple- ζ basis set Def2-TZVP [41,42] and included corrections for dispersion using the D3BJ method [43] and solvation in toluene using PCM [44]. All geometries are supplied as a separate XYZ file.

6.4. Crystallographic Methods

The crystal data for all compounds are compiled in Tables S1–S3. Crystals of **1-Br**, **1-I**, **1-I·THF**, **2** and $(C_5H_4N-S)_2C=C(C_5H_4N-S)_2$ were examined using a Bruker Apex 2000 CCD area detector diffractometer, and data were collected using graphite-monochromated Mo-K α radiation ($\lambda = 0.71073$). Crystals of **1-Cl** were examined using a dual-wavelength [Mo-K α ($\lambda = 0.71073$) or Cu-K α ($\lambda = 1.54178$)] Rigaku FR-X diffractometer with a HyPix 6000HE photon-counting detector. Intensities were integrated from data recorded on 1° frames by ω rotation. A multiscan method (SADABS) [45] or a Gaussian grid faced-indexed absorption correction with a beam profile were applied [46]. The structures were solved using SHELXS [47]; the datasets were refined by full-matrix least-squares on reflections with $F^2 \geq 2\sigma(F^2)$ values, with anisotropic displacement parameters for all non-hydrogen atoms, and with constrained riding hydrogen geometries [48]. Uiso(H) was set at 1.2 (1.5 for methyl groups) times Ueq of the parent atom. The largest features in the final difference syntheses were close to heavy atoms and were of no chemical significance. SHELX [47,48] was employed through OLEX2 for structure solution and refinement [49]. ORTEP-3 [50] and POV-Ray [51] were employed for molecular graphics. The structures have been deposited within the Cambridge Crystallographic Data Centre (CCDC 2088557, 2175279–2175282, 2175291, 2175339). This information can be obtained free of charge from www.ccdc.cam.ac.uk/data_request/cif (accessed on 13 July 2022). Inspection of the data of **1-I·THF** revealed the presence of a non-merohedral twin component accounting for approximately 40% of the reflections. The partially refined data were treated with PLATON TWINROTMAT [52] to separate the two twin components and generate a file containing reflection information from both of them. The structure was then refined against this new reflection file, and the relative scale factor of the two components was refined, converging at a ratio of 0.432(4):0.568(4).

Supplementary Materials: The supporting information can be downloaded at: <https://www.mdpi.com/article/10.3390/molecules27144564/s1>. Figure S1: 1H NMR (400 MHz, 298 K, $CDCl_3$) spectrum of HTptm CF_3 , with assignment. Figure S2: $^{13}C\{^1H\}$ NMR (100 MHz, 298 K, $CDCl_3$) spectrum of HTptm CF_3 , with assignment. Figure S3: $^{13}C\{^1H\}$ NMR (100 MHz, 298 K, $CDCl_3$) spectrum of HTptm CF_3 in the region 110–170 ppm, with assignment. Figure S4: $^{19}F\{^1H\}$ NMR (376 MHz, 298 K, $CDCl_3$) spectrum of HTptm CF_3 . Figure S5: 1H NMR (400 MHz, 298 K, C_6D_6) spectrum of **1-Cl**, with assignment. Figure S6: $^{13}C\{^1H\}$ NMR (125 MHz, 298 K, C_4D_8O) spectrum of **1-Cl**, with assignment. Figure S7: $^{13}C\{^1H\}$ NMR (100 MHz, 298 K, C_6D_6) spectrum of **1-Cl**. Figure S8: 1H NMR (400 MHz, 298 K, C_6D_6) spectrum of **1-Br**, with assignment. Figure S9: $^{13}C\{^1H\}$ NMR (125 MHz, 298 K, C_4D_8O) spectrum of **1-Br**, with assignment. Figure S10: $^{13}C\{^1H\}$ NMR (100 MHz, 298 K, C_6D_6) spectrum of **1-Br**. Figure S11: 1H NMR (400 MHz, 298 K, C_6D_6) spectrum of **1-I**, with assignment. Figure S12: $^{13}C\{^1H\}$ NMR (100 MHz, 298 K, C_6D_6) spectrum of **1-I**, with assignment. Figure S13: 1H NMR (400 MHz, 298 K, C_6D_6) spectrum of **2**, with assignment. Figure S14: $^{13}C\{^1H\}$ NMR (100 MHz, 298 K, C_6D_6) spectrum of **2**, with assignment. Figure S15: 1H NMR (400 MHz, 298 K, C_6D_6/C_4D_8O) spectrum of the NMR scale reaction product of KN'' and HTptm. Figure S16: 1H NMR (400 MHz, 298 K, C_6D_6/C_4D_8O) spectrum in the region 6.0–9.0 ppm of the NMR scale reaction product of KN'' and HTptm. Figure S17: FTIR spectrum of HTptm CF_3 . Figure S18: FTIR spectrum of **1-Cl**. Figure S19: FTIR spectrum of **1-Br**. Figure S20: FTIR spectrum of **1-I**. Figure S21: Crystal structure of **3**. Ellipsoids are set at 50% probability level and hydrogens omitted for clarity. The asymmetric unit contains half a molecule; the full molecule has been reproduced here. Symmetry operation used to generate equivalent atoms: $i = 1-x, 1-y, -z$. C: black; N: blue; S: yellow. Table S1: Crystallographic data for **1-X**. Table S2: Crystallographic data for HTptm CF_3 , **1-I·THF** and **2**. Table S3: Crystallographic data for $(C_5H_4N-S)_2C=C(C_5H_4N-S)_2$. Table S4: Computational data.

Author Contributions: Conceptualization, F.O. and L.S.; methodology, F.O., L.S. and M.P.S.; NMR analysis, V.M.T. and M.P.S.; X-ray crystallography, F.O., M.P.S., I.J.V.-Y. and K.S.; synthesis, M.P.S. and

E.S.; theoretical analysis, L.S.; writing—original draft preparation, M.P.S. and F.O.; writing—review and editing, all authors; funding acquisition, F.O. All authors have read and agreed to the published version of the manuscript.

Funding: This research was funded by the Royal Society (RGS\R2\202097) and Engineering and Physical Sciences Research Council (EP/W00691X/1, EP/T019876/1). X-ray diffraction at Leicester was also supported by the Engineering and Physical Sciences Research Council (EP/V034766/1).

Institutional Review Board Statement: Not applicable.

Informed Consent Statement: Not applicable.

Data Availability Statement: Additional research data supporting this publication are available from Mendeley at doi: 10.17632/694vs8nmgp.3.

Acknowledgments: We thank the University of Leicester and the College of Life Science and Engineering for a PhD scholarship (M.P.S.). We also thank Stuart Macgregor for helpful discussions and suggestions.

Conflicts of Interest: The authors declare no conflict of interest.

Sample Availability: Samples of the compounds **1-Cl**, **1-Br**, **1-I** and **2** are available from the authors.

References

1. Bourget-Merle, L.; Lappert, M.F.; Severn, J.R. The Chemistry of β -Diketiminatometal Complexes. *Chem. Rev.* **2002**, *102*, 3031–3065. [[CrossRef](#)] [[PubMed](#)]
2. Lappert, M.F.; Protchenko, A.; Power, P.; Seeber, A. *Metal Amides*; Wiley: Hoboken, NJ, USA, 2008.
3. Kays, D.L. Extremely bulky amide ligands in main group chemistry. *Chem. Soc. Rev.* **2016**, *45*, 1004–1018. [[CrossRef](#)] [[PubMed](#)]
4. Bigmore, H.R.; Lawrence, S.C.; Mountford, P.; Tredget, C.S. Coordination, organometallic and related chemistry of tris(pyrazolyl)methane ligands. *Dalton Trans.* **2005**, 635–651. [[CrossRef](#)] [[PubMed](#)]
5. Stradiotto, M.; Lundgren, R.J. *Ligand Design in Metal Chemistry: Reactivity and Catalysis*; Wiley: Hoboken, NJ, USA, 2016.
6. Trofimenko, S. Recent advances in poly(pyrazolyl)borate (scorpionate) chemistry. *Chem. Rev.* **1993**, *93*, 943–980. [[CrossRef](#)]
7. Wolf, B.M.; Stuhl, C.; Maichle-Mössmer, C.; Anwender, R. Dimethylcalcium. *J. Am. Chem. Soc.* **2018**, *140*, 2373–2383. [[CrossRef](#)]
8. Westerhausen, M.; Koch, A.; Görls, H.; Kriek, S. Heavy Grignard Reagents: Synthesis, Physical and Structural Properties, Chemical Behavior, and Reactivity. *Chem. Eur. J.* **2017**, *23*, 1456–1483. [[CrossRef](#)]
9. Rauch, M.; Rucolo, S.; Parkin, G. Synthesis, Structure, and Reactivity of a Terminal Magnesium Hydride Compound with a Carbatrane Motif, [Tism^{Pri}Benz]MgH: A Multifunctional Catalyst for Hydrosilylation and Hydroboration. *J. Am. Chem. Soc.* **2017**, *139*, 13264–13267. [[CrossRef](#)]
10. Rauch, M.; Parkin, G. Zinc and Magnesium Catalysts for the Hydrosilylation of Carbon Dioxide. *J. Am. Chem. Soc.* **2017**, *139*, 18162–18165. [[CrossRef](#)]
11. Santo, R.; Miyamoto, R.; Tanaka, R.; Nishioka, T.; Sato, K.; Toyota, K.; Obata, M.; Yano, S.; Kinoshita, I.; Ichimura, A.; et al. Diamagnetic–Paramagnetic Conversion of Tris(2-pyridylthio)methylcopper(III) through a Structural Change from Trigonal Bipyramidal to Octahedral. *Angew. Chem. Int. Ed.* **2006**, *45*, 7611–7614. [[CrossRef](#)]
12. Kinoshita, I.; Wright, L.J.; Kubo, S.; Kimura, K.; Sakata, A.; Yano, T.; Miyamoto, R.; Nishioka, T.; Isobe, K. Design and synthesis of copper complexes of novel ligands based on the pyridine thiolate group. *Dalton Trans.* **2003**, *10*, 1993–2003. [[CrossRef](#)]
13. Miyamoto, R.; Santo, R.; Matushita, T.; Nishioka, T.; Ichimura, A.; Teki, Y.; Kinoshita, I. A complete series of copper(II) halide complexes (X = F, Cl, Br, I) with a novel Cu(II)–C(sp³) bond. *Dalton Trans.* **2005**, *19*, 3179–31866. [[CrossRef](#)] [[PubMed](#)]
14. Kitano, K.; Kuwamura, N.; Tanaka, R.; Santo, R.; Nishioka, T.; Ichimura, A.; Kinoshita, I. Synthesis and characterization of tris(2-pyridylthio)methanido Zn complex with a Zn–C bond and DFT calculation of its one-electron oxidized species. *Chem. Commun.* **2008**, *11*, 1314–1316. [[CrossRef](#)] [[PubMed](#)]
15. Sattler, W.; Parkin, G. Synthesis, Structure, and Reactivity of a Mononuclear Organozinc Hydride Complex: Facile Insertion of CO₂ into a Zn–H Bond and CO₂-Promoted Displacement of Siloxide Ligands. *J. Am. Chem. Soc.* **2011**, *133*, 9708–9711. [[CrossRef](#)]
16. Shannon, R.D. Revised effective ionic radii and systematic studies of interatomic distances in halides and chalcogenides. *Acta Cryst. A* **1976**, *32*, 751–767. [[CrossRef](#)]
17. Sattler, W.; Parkin, G. Structural characterization of zinc bicarbonate compounds relevant to the mechanism of action of carbonic anhydrase. *Chem. Sci.* **2012**, *3*, 2015–2019. [[CrossRef](#)]
18. Sattler, W.; Rucolo, S.; Parkin, G. Synthesis, Structure, and Reactivity of a Terminal Organozinc Fluoride Compound: Hydrogen Bonding, Halogen Bonding, and Donor–Acceptor Interactions. *J. Am. Chem. Soc.* **2013**, *135*, 18714–18717. [[CrossRef](#)] [[PubMed](#)]
19. Stuhl, C.; Maichle-Mössmer, C.; Anwender, R. Magnesium Stung by Nonclassical Scorpionate Ligands: Synthesis and Cone-Angle Calculations. *Chem. Eur. J.* **2018**, *24*, 14254–14268. [[CrossRef](#)] [[PubMed](#)]
20. Poater, A.; Cosenza, B.; Correa, A.; Giudice, S.; Ragone, F.; Scarano, V.; Cavallo, L. SambVca: A Web Application for the Calculation of the Buried Volume of N-Heterocyclic Carbene Ligands. *Eur. J. Inorg. Chem.* **2009**, *2009*, 1759–1766. [[CrossRef](#)]

21. Falivene, L.; Cao, Z.; Petta, A.; Serra, L.; Poater, A.; Oliva, R.; Scarano, V.; Cavallo, L. Towards the online computer-aided design of catalytic pockets. *Nat. Chem.* **2019**, *11*, 872–879. [[CrossRef](#)]
22. Guzei, I.A.; Wendt, M. An improved method for the computation of ligand steric effects based on solid angles. *Dalton Trans.* **2006**, *33*, 3991–3999. [[CrossRef](#)]
23. Clavier, H.; Nolan, S.P. Percent buried volume for phosphine and *N*-heterocyclic carbene ligands: Steric properties in organometallic chemistry. *Chem. Commun.* **2010**, *46*, 841–861. [[CrossRef](#)] [[PubMed](#)]
24. Ortu, F.; Moxey, G.J.; Blake, A.J.; Lewis, W.; Kays, D.L. Tuning Coordination in s-Block Carbazol-9-yl Complexes. *Chem. Eur. J.* **2015**, *21*, 6949–6956. [[CrossRef](#)] [[PubMed](#)]
25. Brand, S.; Causero, A.; Elsen, H.; Pahl, J.; Langer, J.; Harder, S. Ligand Effects in Calcium Catalyzed Ketone Hydroboration. *Eur. J. Inorg. Chem.* **2020**, *2020*, 1728–1735. [[CrossRef](#)]
26. De Castro, V.D.; de Lima, G.M.; Filgueiras, C.A.L.; Gambardella, M.T.P. The molecular structure and spectral studies of mercaptopyridyl-based ligands. *J. Mol. Struct.* **2002**, *609*, 199–203. [[CrossRef](#)]
27. Chakrabarti, N.; Sattler, W.; Parkin, G. Structural characterization of *tris*(pyrazolyl)hydroborato and *tris*(2-pyridylthio)methyl lithium compounds: Lithium in uncommon trigonal pyramidal and trigonal monopyramidal coordination environments. *Polyhedron* **2013**, *58*, 235–246. [[CrossRef](#)]
28. Kuwamura, N.; Kato, R.; Kitano, K.; Hirotsu, M.; Nishioka, T.; Hashimoto, H.; Kinoshita, I. Carbene–carbanion equilibrium for *tris*(2-pyridylthio)methanido Fe(II) complexes. *Dalton Trans.* **2010**, *39*, 9988–9993. [[CrossRef](#)] [[PubMed](#)]
29. Goodwin, C.A.P.; Smith, A.; Ortu, F.; Vitorica-Yrezabal, I.J.; Mills, D.P. Salt metathesis versus protonolysis routes for the synthesis of silylamide Hauser base (R_2NMgX ; X = halogen) and amido-Grignard (R_2NMgR) complexes. *Dalton Trans.* **2016**, *45*, 6004–6014. [[CrossRef](#)]
30. Stevens, M.P.; Spray, E.; Vitorica-Yrezabal, I.J.; Singh, K.; Timmermann, V.M.; Sotorrios, L.; Macgregor, S.A.; Ortu, F. Synthesis, Characterisation and Reactivity of Group 2 Complexes with a Thiopyridyl Scorpionate Ligand. *Dalton Trans.* **2022**. *accepted manuscript*. [[CrossRef](#)]
31. Kloubert, T.; Müller, C.; Kriek, S.; Schlotthauer, T.; Görls, H.; Westerhausen, W. 3-(2-Pyridyl)-5-(2-thienyl)pyrazole and Complexes of Its Anion with Lithium, Magnesium, Calcium, and Zinc Ions. *Eur. J. Inorg. Chem.* **2012**, *2012*, 5991–6001. [[CrossRef](#)]
32. Kanischchev, O.S.; Dolbier, W.R. Synthesis and Characterization of 2-Pyridylsulfur Pentafluorides. *Angew. Chem. Int. Ed.* **2015**, *54*, 280–284. [[CrossRef](#)]
33. Schlosser, M.; Hartmann, J. Transmetalation and Double Metal Exchange: A Convenient Route to Organolithium Compounds of the Benzyl and Allyl Type. *Angew. Chem. Int. Ed.* **1973**, *12*, 508–509. [[CrossRef](#)]
34. Frisch, M.J.; Trucks, G.W.; Schlegel, H.B.; Scuseria, G.E.; Robb, M.A.; Cheeseman, J.R.; Scalmani, G.; Barone, V.; Petersson, G.A.; Nakatsuji, H.; et al. *Gaussian 16, Revision A.03*; Gaussian Inc.: Wallingford, CT, USA, 2016.
35. Becke, A.D. Density-functional exchange-energy approximation with correct asymptotic behavior. *Phys. Rev. A* **1988**, *38*, 3098–3100. [[CrossRef](#)] [[PubMed](#)]
36. Perdew, J.P. Density-functional approximation for the correlation energy of the inhomogeneous electron gas. *Phys. Rev. B* **1986**, *33*, 8822–8824. [[CrossRef](#)] [[PubMed](#)]
37. Andrae, D.; Häußermann, U.; Dolg, M.; Stoll, H.; Preuß, H. Energy-adjusted *ab initio* pseudopotentials for the second and third row transition elements. *Theor. Chim. Acta* **1990**, *77*, 123–141. [[CrossRef](#)]
38. Hehre, W.J.; Ditchfield, R.; Pople, J.A. Self-Consistent Molecular Orbital Methods. XII. Further Extensions of Gaussian-Type Basis Sets for Use in Molecular Orbital Studies of Organic Molecules. *J. Chem. Phys.* **1972**, *56*, 2257–2261. [[CrossRef](#)]
39. Hariharan, P.C.; Pople, J.A. The influence of polarization functions on molecular orbital hydrogenation energies. *Theor. Chim. Acta* **1973**, *28*, 213–222. [[CrossRef](#)]
40. Höllwarth, A.; Böhme, M.; Dapprich, S.; Ehlers, A.W.; Gobbi, A.; Jonas, V.; Köhler, K.F.; Stegmann, R.; Veldkamp, A.; Frenking, G. A set of d-polarization functions for pseudo-potential basis sets of the main group elements Al–Bi and f-type polarization functions for Zn, Cd, Hg. *Chem. Phys. Lett.* **1993**, *208*, 237–240. [[CrossRef](#)]
41. Weigend, F.; Ahlrichs, R. Balanced basis sets of split valence, triple zeta valence and quadruple zeta valence quality for H to Rn: Design and assessment of accuracy. *Phys. Chem. Chem. Phys.* **2005**, *7*, 3297–3305. [[CrossRef](#)]
42. Weigend, F.; Köhn, A.; Hättig, C. Efficient use of the correlation consistent basis sets in resolution of the identity MP2 calculations. *J. Chem. Phys.* **2002**, *116*, 3175–3183. [[CrossRef](#)]
43. Grimme, S.; Ehrlich, S.; Goerigk, L. Effect of the damping function in dispersion corrected density functional theory. *J. Comput. Chem.* **2011**, *32*, 1456–1465. [[CrossRef](#)]
44. Tomasi, J.; Mennucci, B.; Cammi, R. Quantum Mechanical Continuum Solvation Models. *Chem. Rev.* **2005**, *105*, 2999–3093. [[CrossRef](#)] [[PubMed](#)]
45. Sheldrick, G. *SADABS: Program for Absorption Correction Using Area Detector Data*; University of Göttingen: Göttingen, Germany, 1996.
46. *CrysAlisPRO*, Version 39.27b; Oxford Diffraction/Agilent Technologies UK Ltd.: Yarnton, UK, 2017.
47. Sheldrick, G. A short history of SHELX. *Acta Cryst. Sect. A* **2008**, *64*, 112–122. [[CrossRef](#)] [[PubMed](#)]
48. Sheldrick, G.M. Crystal structure refinement with SHELXL. *Acta Crystallogr. Sect. C* **2015**, *71*, 3–8. [[CrossRef](#)] [[PubMed](#)]
49. Dolomanov, O.V.; Bourhis, L.J.; Gildea, R.J.; Howard, J.A.K.; Puschmann, H. OLEX2: A complete structure solution, refinement and analysis program. *J. Appl. Crystallogr.* **2009**, *42*, 339–341. [[CrossRef](#)]

50. Farrugia, L.J. WinGX and ORTEP for Windows: An update. *J. Appl. Crystallogr.* **2012**, *45*, 849–854. [[CrossRef](#)]
51. *POV-Ray Persistence of Vision Raytracer*, Version 3.7; Pty. Ltd.: Williamston, Australia, 2013.
52. Spek, A.L. Single-crystal structure validation with the program *PLATON*. *J. Appl. Crystallogr.* **2003**, *36*, 7–13. [[CrossRef](#)]